# Using the Constant Properties Model for accurate Performance Estimation of Thermoelectric Generator Elements

P. Ponnusamy[1], J. de Boor[1] and E. Müller[1,2]

[1]German Aerospace Center (DLR), Institute of Materials Research, D–51170 Köln, Germany

[2]Justus Liebig University Gießen, Institute of Inorganic and Analytical Chemistry, D–35392 Gießen, Germany

## Abstract

Thermoelectric devices convert thermal energy directly into electrical energy or vice versa. Analytically, the performance (efficiency and power output) of a thermoelectric generator can be quickly estimated using a Constant Properties Model (CPM) suggested by Ioffe. However, material properties in general are temperature dependent and the CPM can yield meaningful estimates only if the constant values of the TE properties used in the formulations are physically appropriate. In this study, a comparison of different averaging modes shows that a combination of integral averaging over the temperature scale for the Seebeck coefficient and spatial averages for the electrical and thermal resistivities proves to be the best among the considered approximations to represent the constant property values. However, averaging spatially requires the knowledge of the exact temperature distribution along the length of the thermoelectric leg (temperature profile), which is usually obtained by Finite Element Method (FEM) calculations. Since FEM is costly and time consuming, a fast and easy way of obtaining a well approximated self-consistent temperature profile is used in this study. The relevance, magnitude and the physical origin of the non-linearity of the temperature profile are visualised by separately plotting the individual contributions to the bending of the temperature profile (Joule, Thomson and Fourier heat contributions). On analyzing the temperature profiles for different highly efficient thermoelectric materials, it is found that the non-constancy of the temperature dependence of the thermal conductivity significantly contributes to the deflection of real temperature profiles from a linear one. This mainly explains the considerable discrepancy of CPM results from exact calculations whereas, so far, the neglect of Thomson heat has been assumed to be the main source

of discrepancy and several models with Thomson correction factors have been proposed. With our current view, such models cannot completely remove the discrepancy to CPM unless the *T* profile is taken into account and can lead to unpredictable error for different material cases and temperatures.

**Keywords**: TEG performance, Device modeling, Temperature profile, Constant properties model, Fourier heat, Thomson heat.

# 1 Introduction

Thermoelectric generator (TEG) materials work by converting a certain fraction of the heat passed through them into useful electrical power, involving interplay of the transport of charge and heat in the solid state. Typically, a thermoelectric (TE) module consists of a series of pairs of legs made of n- and p-type semiconductor material, electrically connected in series and thermally in parallel [1]. Consider a single TE leg of length $L$ as shown in Figure 1, supplied with a constant hot side temperature of $T_{\mathrm{h}}$ and a cold side temperature of $T_{\mathrm{c}}$, where $\Delta T = T_{\mathrm{h}} - T_{\mathrm{c}}$.

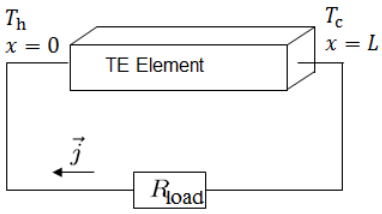


**Figure 1: Schematic showing a TE leg connected in a circuit to an external load resistor. At open loop ($j = 0$), only Fourier heat is flowing whereas in non-zero current case additionally Joule, Peltier and Thomson heat are involved ($j$ – current density).**

At open circuit condition, the heat flow entering at the hot side ($Q_{\mathrm{in}}$) is the same as the heat flow leaving at the cold side ($Q_{\mathrm{out}}$) and no electrical power is generated. But, when the TE leg is connected to a load as shown in Figure 1, current $I = jA$ ($j$ is the current density and $A$ is the area of cross section) flows in this closed circuit due to the generated thermoelectric voltage and a part of the input heat, equivalent to $Q_{\mathrm{in}} - Q_{\mathrm{out}}$ is converted into the thermoelectric power $P$ [2].

$$P = Q_{\mathrm{in}} - Q_{\mathrm{out}} = V \cdot I, \text{ where } V = V_o - R_{\mathrm{in}} I, \quad V_o = \alpha \Delta T \tag{1}$$

Here, $V$ is the output voltage at the TE leg which is given by the Seebeck voltage generated $V_{\mathrm{o}}$ (the maximum output voltage, reached at open loop) minus the voltage drop due to internal resistance ($R_{\mathrm{in}}$) of the TE material ($R_{\mathrm{in}} = \rho L/A$, where $\rho$ is the electrical resistivity of the TE material, $L$ – length). The material properties, $\alpha$ (Seebeck coefficient) and $\rho$ are generally temperature dependent and hence the overall Seebeck voltage $V_{\mathrm{o}}$ and the net internal resistance ($R_{\mathrm{in}}$) are calculated by integrating over temperature and length, respectively, *i.e.*, $V_{\mathrm{o}} = \int_{T_c}^{T_{\mathrm{h}}} \alpha(T) dT$ and $R_{\mathrm{in}} = \int_0^L \rho\big(T(x)\big) dx/A$. Here, $T(x)$ is the temperature profile (temperature distribution along the length of the TE leg).

Like for any thermodynamic machine, the efficiency ($\eta$) of a thermoelectric generator (TEG) is given by the ratio of output power ($P$) to the input heat flow ($Q_{\mathrm{in}}$).

$$\eta = P/Q_{\mathrm{in}} \tag{2}$$

Here,

$$Q_{\mathrm{in}} = -\kappa_{\mathrm{h}} \cdot A \cdot \frac{dT}{dx_{\mathrm{h}}} + I \cdot \alpha_{\mathrm{h}} \cdot T_{\mathrm{h}} \tag{3}$$

which is the heat input at the hot side, split into the Fourier heat flow $-\kappa_{\mathrm{h}} \cdot A \cdot \frac{dT}{dx_{\mathrm{h}}}$ (including contributions to balance the Joule and Thomson heat released in the element) plus the absorbed Peltier heat flow $I \cdot \alpha_{\mathrm{h}} \cdot T_{\mathrm{h}}$ ($\kappa$ being the thermal conductivity). Please note that $Q_{\mathrm{in}}, Q_{\mathrm{out}}$, $-\kappa_{\mathrm{h}} A \frac{dT}{dx_{\mathrm{h}}}$, $I\alpha_{\mathrm{h}}T_{\mathrm{h}}$ are formally heat flows [W]. The suffix h denotes the hot side values, with $\kappa_{\mathrm{h}} = \kappa(T_{\mathrm{h}})$ and $\alpha_{\mathrm{h}} = \alpha(T_{\mathrm{h}})$. Here, it is noteworthy that the gradient of $T(x)$ *i.e.*, $\frac{dT}{dx}$ is required for determining $Q_{\mathrm{in}}$ and, thus, the efficiency. $T(x)$ is obtained by solving the thermoelectric heat balance equation, which is a second order non-linear partial differential equation, written in 1D as,

$$\kappa(T)\frac{\boldsymbol{\partial^2 T}}{\boldsymbol{\partial x^2}} + \frac{d\kappa}{dT}\left(\frac{\boldsymbol{\partial T}}{\boldsymbol{\partial x}}\right)^{\mathbf{2}} - jT\frac{d\alpha}{dT}\frac{\boldsymbol{\partial T}}{\boldsymbol{\partial x}} = -\rho(T)j^2 \tag{4}$$

This equation is obtained from the physical implication that the divergence of flowing Fourier heat equals the sum of locally appearing Joule heat and Thomson heat [2]. Thomson heat is fundamentally the consequence of the local heat balance when flowing Peltier heat within the TE leg changes with local temperature variation due to the temperature dependence of the Seebeck coefficient $\alpha(T(x))$. Exchanged Peltier heat at the junctions of the n or p leg which is the difference of the inflowing and outflowing Peltier heat – to be distinguished from the flowing Peltier heat itself, $I \cdot \alpha \cdot T$, flowing at any point of a thermoelectric circuit – is considered as an additional heat input as in Eq. (3) and is relevant for the estimation of efficiency but is furthermore not affecting the shaping of the temperature profile. Here, $\tau$ is the Thomson coefficient which is given by $T\frac{\partial \alpha}{\partial T}$ [3]. In a strict case (incorporating the T dependence of the material properties $\alpha$, $\kappa$ and $\sigma$), the accurate $T(x)$ can be obtained by solving Eq. (4) using numerical methods like Finite Element Methods (FEM) [4, 5], Finite Volume Methods (FVM) [6-8] or Finite Difference Methods (FDM) [5] and according numerical tools [9, 10]. These

solution methods are time consuming and costly and are impractical for parameter studies if the geometry is varied as is intended for computational TEG module design.

On the contrary, in order to quickly estimate the electrical output power and the conversion efficiency of a TEG, a constant property model (CPM) suggested by Ioffe is often used [3]. But, the question of selection of appropriately averaged values [11-15] for the TE properties to be used in the CPM formulae has not been answered clearly yet. Practically, averaging of the properties over the temperature scale of the range of operation (temperature averaging – in the following denoted by TAv) is the easiest and accordingly has been used already from Ioffe's times [3]. It has been shown to work well for certain materials [2, 5, 9, 16]. Nevertheless, the error involved in such an approximation can be high depending on the chosen temperature range and the temperature dependence of the material [5, 12, 15, 17], as will be shown in this work. So far, the neglect of Thomson heat and the Joule heat asymmetry are generally assumed to be the reasons why CPM deviates from exact results and hence, there are many publications on the importance of Thomson heat [18-21]. But, a clear conclusion has not been achieved yet nor has a suitable average been proposed that can be used universally for all materials and boundary conditions.

Apart from CPM, there are also simplified models based on assuming different analytical formulations for the $T$ dependencies of the material properties [16, 22-24] and/or different mathematical functions for $T(x)$ [25-27]. For example, recently, Ryu *et al*.[24] suggested an interesting model based on the exact theory, with linear assumption of $\alpha(T)$ and $\kappa\rho(T)$ which holds good for most of the thermoelectric materials. Some models are based on electrical analogy of thermal flow [28], some assume a constant Thomson coefficient [29, 30] and some assuming different mathematical functions for the Thomson heat [19, 31]. However, these are again approximate methods applicable for specific materials and for certain temperature ranges. On similar lines, recently, a novel definition of a technologically relevant figure of merit $ZT_{\mathrm{eng}}$ has been suggested by Kim *et al.* [12], but here again temperature averages are used to compensate for the 'missing' Thomson heat in CPM [14, 32].

In addition to the above, the excel calculator by Snyder *et al.* [2, 33] based on Finite Difference Method (FDM), provides fast and accurate results with reduced variables based on the compatibility approach. But, the temperature profile, which is significant for understanding the

working of a TE element, is not calculated explicitly in this approach and since the calculations are in terms of reduced current, a direct picture of the different TE effects taking place in the leg is not easily visualised. Moreover, the calculation is no more straightforward when thermal and electrical contact resistances have to be considered in the calculation.

In this study, the degree of universality of existing averaging methods for CPM is analysed on material classes with different *T* dependence, selected based on low, medium and mid-high temperature operations and physically appropriate averages to be used with CPM are proposed. By analysing the individual contributions to the temperature profile, we will demonstrate how the TE performance estimation using CPM deviates unpredictably in different material cases and different operating temperature ranges when conventional averaging methods are used. Further, based on the temperature profiles, we will explain when and why CPM works and why it fails in some cases.

# 2 Methods and results

## 2.1 Estimation of TE performance by CPM

According to the Constant Properties Model (CPM) suggested by Ioffe [3], accumulated heat at the hot and cold sides is given by,

$$Q_{\mathrm{in}} = Q_{\mathrm{h}} = K\Delta T + \alpha T_{\mathrm{h}} I - \frac{1}{2} R_{\mathrm{in}} I^2 \quad \text{and} \quad Q_{\mathrm{out}} = Q_{\mathrm{c}} = K\Delta T + \alpha T_{\mathrm{c}} I + \frac{1}{2} R_{\mathrm{in}} I^2 \qquad (5)$$

Here $K$ is the thermal conductance given by $\frac{\kappa A}{L}$. $K\Delta T$ corresponds to the average Fourier heat flow along the element, $\alpha T_{\mathrm{h}} I$ and $\alpha T_{\mathrm{c}} I$ are the absorbed and released Peltier heat and $R_{\mathrm{in}} I^2$ is the Joule heat released in the leg which overlays the average Fourier heat flow, being transported by half to each of the hot and cold sides, respectively. The maximum efficiency $\eta_{\max}$ of a TE leg is obtained from the above equations (substituting Eq. (5) in Eq.(2)) and is given by,

$$\eta_{max} = \frac{\Delta T}{T_h} \frac{\left(-1 + \sqrt{1 + zT_m}\right)}{\left(\frac{T_c}{T_h} + \sqrt{1 + zT_m}\right)} \qquad (6)$$

where $\frac{\Delta T}{T_\mathrm{h}}$ is the Carnot efficiency and $zT_\mathrm{m}$ is the dimensionless figure of merit at the mean temperature $T_\mathrm{m} = \frac{T_\mathrm{h}+T_\mathrm{c}}{2}$, defined as $\frac{\alpha^2\sigma}{\kappa} \cdot T_\mathrm{m}$. The maximum electrical power output using CPM is given by ($P = Q_\mathrm{in} - Q_\mathrm{out}$),

$$P_\mathrm{max} = \alpha^2 \frac{\Delta T^2}{4\rho L} A \tag{7}$$

where $\alpha^2\sigma$ is called the thermoelectric power factor. The constant property values $\alpha, \sigma$ and $\kappa$ have to be obtained from the temperature dependent TE data by averaging. The following are the most common averaging methods currently in practice [3, 12, 14, 15] – here, $p$ indicates any of the three thermoelectric properties $\alpha, \sigma$ and $\kappa$.

1. Temperature average (TAv): $p_\mathrm{TAv} = \frac{1}{\Delta T}\int_{T_\mathrm{c}}^{T_\mathrm{h}} p(T)dT$, also applied for averaging $zT$: $(zT)_\mathrm{TAv} = \frac{1}{\Delta T}\int_{T_\mathrm{c}}^{T_\mathrm{h}} z(T)TdT$

2. Function value at mean temperature $T_\mathrm{m}$ (FMT) (i.e., $zT_\mathrm{m}$): $p_{T_\mathrm{m}} = p(T_\mathrm{m})$

3. Mean of the function values at the boundary temperatures (MVBT):
$$p_\mathrm{m} = \frac{p(T_\mathrm{h})+p(T_\mathrm{c})}{2} = \frac{p_\mathrm{h}+p_\mathrm{c}}{2}$$

4. Weighted average introduced by Ioffe (IWAv*):* $p_\mathrm{Iwav} = \frac{1}{ln\left({}^{T_\mathrm{h}}/_{T_\mathrm{c}}\right)}\int_{T_\mathrm{c}}^{T_\mathrm{h}} \frac{p(T)}{T}\,dT$

Assuming a continuous curve of a temperature dependence $p(T)$ which can be represented by an appropriate fit to experimental data points, the above averages can be numerically calculated. Since resistances (but not conductances) add up in series, for finding the integral average value for $\kappa$, $1/\kappa(T)$ was used. Likewise, the electrical resistivity $\rho$ is averaged to obtain the CPM value of $\rho(T)$. Figure 2a shows the constant material property values obtained from the averaging techniques 1–4 (above) along with the temperature dependent data for an n-type $Mg_2(Si,Sn)$ sample [34]. Third order polynomial fits were used for this material to approximate the temperature curves of all properties. For such a material with nearly linear $T$ dependence, all the averages are located close together. For a material with

strongly temperature dependent properties like the p-type $Mg_2(Si,Sn)$ shown in Figure 2b, the choice of an appropriate average is not straightforward as can be seen from the figure. 5$^{th}$ order polynomial fits were used for this material.

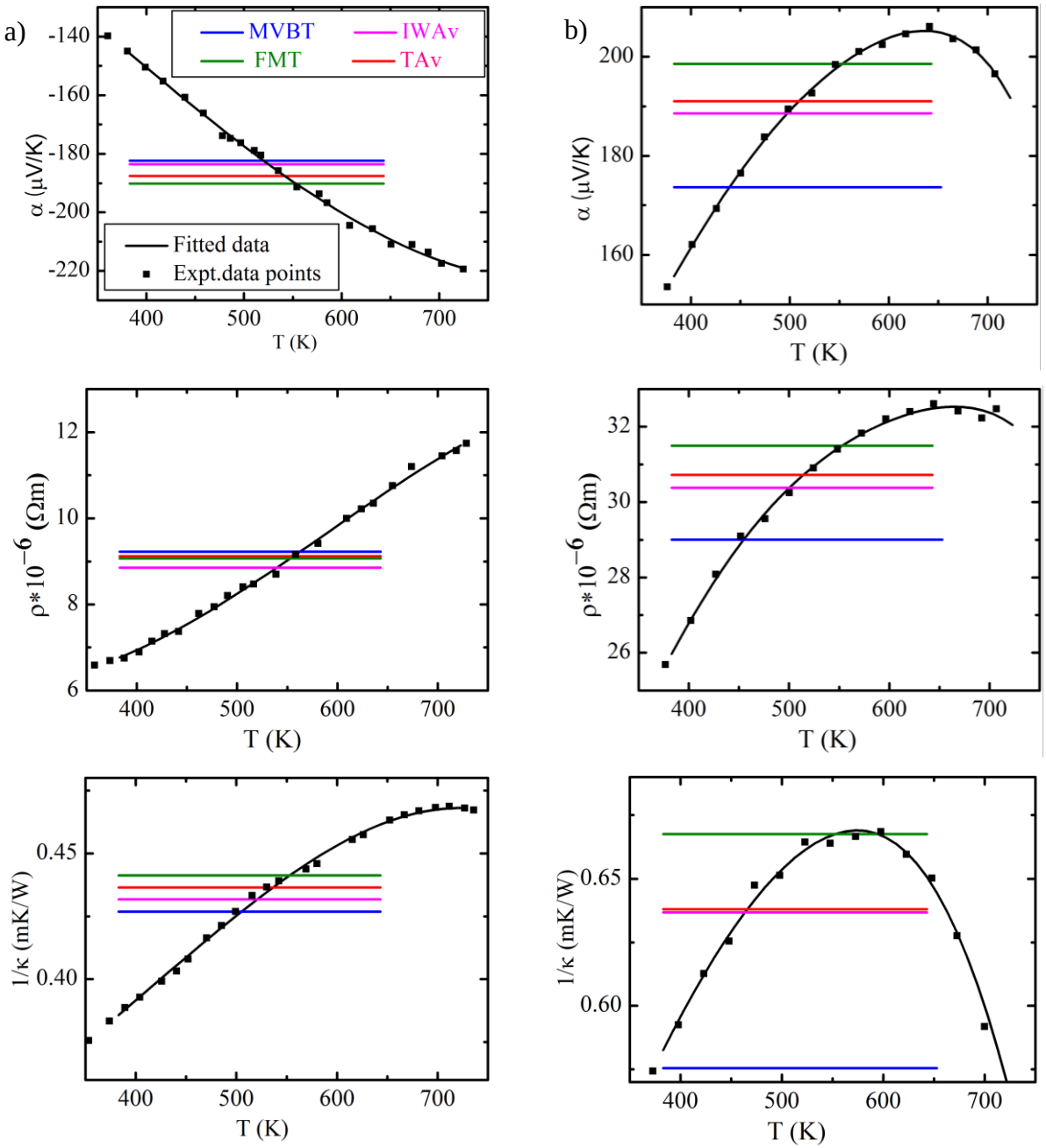


**Figure 2: Graphical representation of different averages along with the *T*-dependent material data for a) n-type $Mg_2(Si,Sn)$ [34] and b) p-type $Mg_2(Si,Sn)$ [35]. The legend for all the graphs is given on the top left diagram. $T_c$ = 383 K and $T_h$ = 723 K.**

By calculating $z$ for each of the above averaging methods from the individually averaged properties (except for the $(zT)_{TAv}$ case where $zT$ curve is directly averaged) for different material

classes, the maximum efficiency using CPM formulation (Eq. 6) was calculated. The material data were taken from literature [34-37] (given in Appendix A). Figure 3 shows a comparison of the maximum efficiency calculated using the CPM formulation, with the exact results calculated using a Finite Element Method (calculated using Ansys 17.0 with a converged mesh size). As can be seen, none of the above considered averages are consistent in predicting the exact performance (Figure 3a). TAv – considered to be the best averaging technique so far [2] – could involve an error as high as 5-16% for strongly temperature dependent materials as seen. Moreover, there is no consistency in over-prediction or under-estimation of performance with different averaging methods except that TAv and TAv($zT$) seem to always overestimate efficiency. In order to overcome this, a combination of spatial averages for resistivities and TAv for Seebeck coefficient was studied as these are physically closest to Ioffe's definition (Eq.(5)) i.e, SpAv of ρ and 1/κ and TAv of α are the physically correct representations of the device parameters $R_{in}$, $K$ and α, which Ioffe's derivation of TE device performance is based upon.

The spatial average of a temperature dependent quantity $p$ [3, 24, 29] is given by

$$p_{\mathrm{SpAv}} = \frac{1}{L}\int_0^L p(T(x))\mathrm{d}x \ . \tag{8}$$

Since resistances add spatially, spatial averaging is physically appropriate for thermal and electrical resistivities. Hence, as can be seen from Figure 3b, performance prediction is within an error of 1.5%, much better than any of the other averaging methods. However, calculation of the spatial averages requires knowledge of the exact temperature profile $T(x)$. The results shown here are calculated with the temperature profiles corresponding to the optimum $j$ in the temperature dependent case, obtained with FEM (Ansys 17.0) which is again time-consuming. $j_{\mathrm{opt}}$ is obtained by calculating $\eta$ for current denisites in the range of the CPM $j_{\mathrm{opt}}$ (calculated using TAv), for the temperature dependent case, fitting a polynomial for $\eta$ and finding the $j$ corresponding to the maximum $\eta$ (the point where $\frac{d\eta}{dj}$ becomes zero). In order to find $T(x)$ quickly, an intuitive way of obtaining the temperature profile through numerical integration is presented in Appendix B. The T profile is obtained iteratively by integration using a linear $T$ profile as a starting solution.

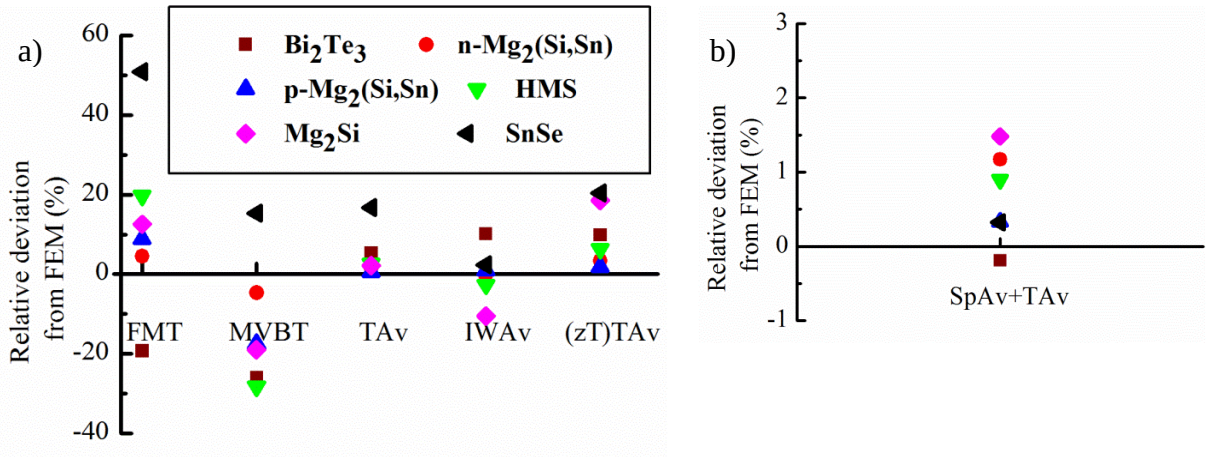


**Figure 3: Comparison of maximum efficiency calculated using different averages in CPM formulation (Eq.(6)): a) FMT, MVBT, TAv, IWAv and (zT)TAv and b) SpAv for resistivities and TAv for Seebeck coefficient, as a comparison with FEM results for six representative TE materials.**

# 3 Discussion

## 3.1 Influence of temperature dependence of material properties

In thermoelectrics, the temperature profile plays a significant role in reliably predicting the performance parameters as outlined in the introduction. Each term in Eq. (4 corresponds to the influence of one out of the three main thermoelectric properties $\kappa(T)$, $\rho(T)$ and $\alpha(T)$ in the heat balance $i.e$,

- Fourier heat flow along the leg due to the applied $\Delta T$ between the hot and cold sides which leads to a significant bow of the temperature profile if the thermal conductivity varies with temperature,
- Joule heat release due to internal resistance $\rho(x)j^2$ which is locally distributed along the length $x$ of the TE leg, and
- similarly, Thomson heat due to the $T$ dependence of the Seebeck coefficient $\alpha(T)$ amounting to $jT\frac{\boldsymbol{d\alpha}}{dT}\frac{dT}{\boldsymbol{dx}}$ (which is physically a distributed Peltier effect due to the temperature gradient and the temperature dependence of the Seebeck coefficient) which causes a locally distributed source or sink of heat along $x$.

Two main aspects governing the curvature of the $T$ profile in a real case are local heat generation/absorption (due to Joule and Thomson effects) and heat redistribution by conduction

(obeying Fourier's law), both depending on the temperature dependence of the material properties ($\rho(T)$ $\alpha(T)$, and $\kappa(T)$). The local Joule heat and Thomson heat that are generated at each point are being transported by Fourier conduction, each making up an individual contribution to the bow of the temperature profile. According to the magnitude of current passing through the TE leg, the temperature profile will vary due to the current-dependent contributions from Joule and Thomson heat. Hence, the material properties $p(T(x))$, vary locally according to the $T(x)$ for each current.

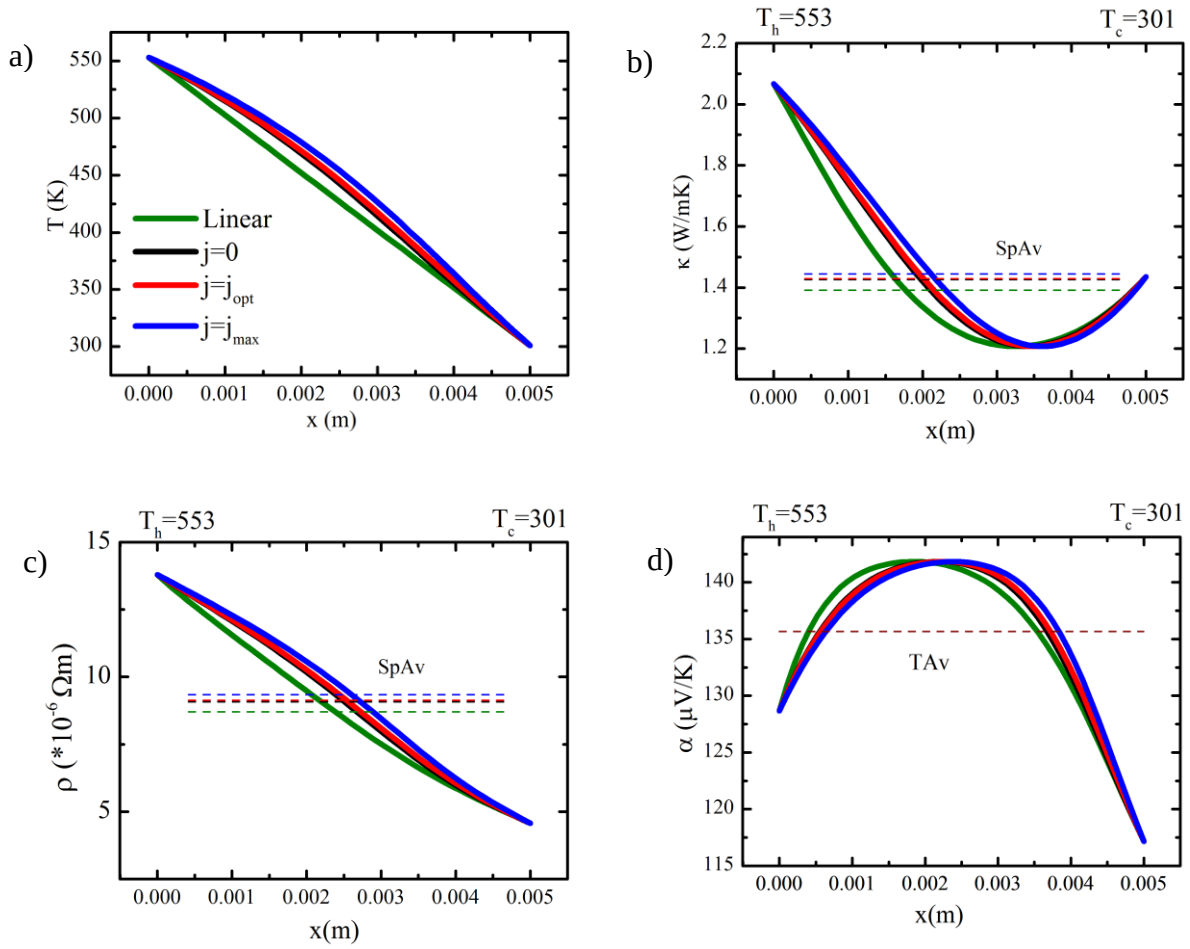


**Figure 4: a) Temperature profiles and the corresponding variation of the TE properties b) Thermal conductivity c) Electrical resistivity d) Seebeck coefficient, along the TE leg for p-type $Bi_2Te_3$. Spatial averages for the resistivities and temperature average for the Seebeck coefficient are shown as horizontal dashed lines.**

For visualization, the temperature profiles and the corresponding material property profiles $p(x)$ for different current flow cases (open circuit, $j_{\mathrm{opt}}$ and $j_{\mathrm{max}}$) in p-type $Bi_2Te_3$ are shown in Figure 4. Here, $j_{\mathrm{max}}$ indicates the maximum current density at which the output voltage vanishes and no

more thermoelectric power output is obtained, *i.e.*, when $V_o = R_{\text{in}} I$. The spatial averages (for resistivities) and the temperature average of the Seebeck coefficient which represent effective constant material properties are indicated as horizontal dashed lines.

The spatial average for a linear $T$ profile is the same as the temperature average. Hence, the difference between TAv and SpAv is illustrated by comparing the green (lowest, in our example) dashed lines to the other ones, consequently leading to different performance predictions as seen in Figure 3.

As can be seen for this material, for the $j = 0$ case the temperature profile is significantly bent compared to the linear $T$ profile. This implies that the temperature dependence of $\kappa(T)$ significantly contributes to the bending of the temperature profile in this material and for this particular temperature range. Since Joule and Thomson heat contribute only slightly to the bending of T profile, the red and blue curves (corresponding to Joule and Thomson heat respectively) are bent only slightly further. This can be verified by visualizing the partial contributions to the $T$ profile (see integration method in Appendix B). By considering the terms corresponding to $\kappa(T)$, Joule heat and Thomson heat separately and equating to $\kappa(T)\frac{\partial^2 T}{\partial x^2}$, the temperature profiles corresponding to the individual contribution are obtained by double integration. The exact $\kappa(x)$, $\rho(x)$ and $\alpha(x)$ at $j_{\text{opt}}$were used.

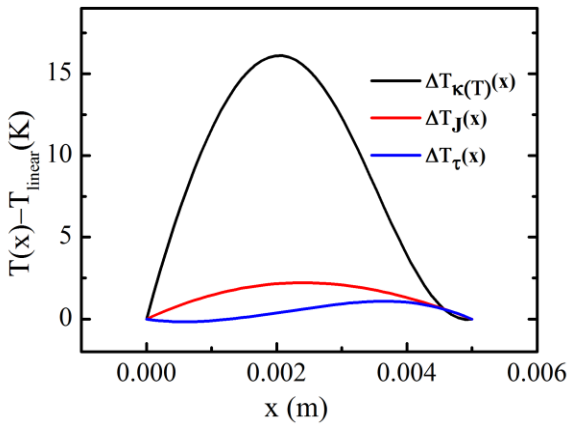


**Figure 5: Partial contributions to the bending of the temperature profile for p-type $Bi_2Te_3$. $\Delta T_{\kappa(T)}(x)$, $\Delta T_{\tau}(x)$ and $\Delta T_{J}(x)$ indicate the contributions due to the $T$ dependence of the thermal conductivity, Thomson heat and Joule heat, respectively. For better readability, the linear part of the temperature profile has been subtracted here.**

Figure 5 shows the individual contributions to the deviation from a linear $T$ profile for p-type $Bi_2Te_3$ at optimum current (maximum efficiency operation). The results are in accordance with the spatial profiles of the temperature dependent material properties (Figure 4). The contribution due to non-constancy of $\kappa(T)$ is positive ($T$ profile bending above the linear $T$ profile) since $\kappa$ is higher at the hot side than at the cold side. Joule and Thomson heat generated (or absorbed) are carried away from their points of generation (or towards their locations of absorption) forming partial $T$ gradients which overlay the open loop temperature profile. Thomson heat, as depends on the slope of the $\alpha(T)$ curve, is negative (will be absorbed) at the warmer section of the leg, becomes zero at the $\alpha$ peak and is released in the colder part as can be read from the blue curve in Figure 5.

## 3.2 Insight into the discrepancy with CPM

In the CPM, Eq. (4) reduces to

$$\kappa \frac{\mathrm{d}^2 T}{\mathrm{d}x^2} = -\rho j^2 \tag{9}$$

giving a temperature profile as

$$T(x) = T_\mathrm{h} + (T_\mathrm{c} - T_\mathrm{h})\frac{x}{L} + \frac{\rho j^2}{2\kappa} x(L - x) \tag{10}$$

which consists only of the linear part $T_\mathrm{h} + (T_\mathrm{c} - T_\mathrm{h})\frac{x}{L}$ due to Fourier heat assuming a constant $\kappa$ and the parabolic part $\frac{\rho j^2}{2\kappa}\boldsymbol{x}(L - \boldsymbol{x})$ due to Joule heat [2], neglecting the actual bending due to $\kappa(T)$. For p-type $Bi_2Te_3$, a comparison of the actual $T$ profile (with temperature dependent material data as input) to the CPM $T$ profile (Eq. (10) using spatially averaged $\rho$ and $\kappa$) can be seen in Figure 6 at $j = j_\mathrm{opt}$, where clearly the CPM temperature profile is quite close to a linear curve but far from the actual T profile obtained by FEM.

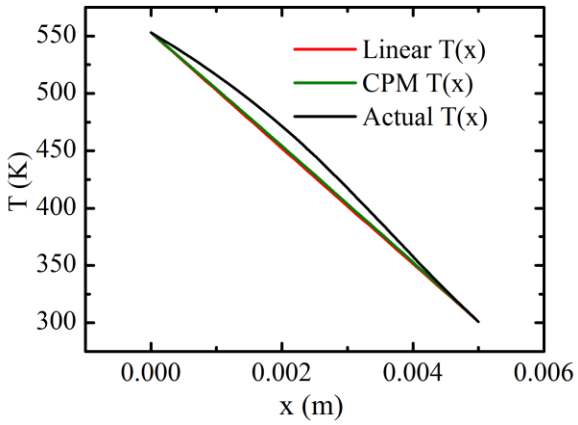


**Figure 6: Linear, CPM and the actual temperature profiles for p-type $Bi_2Te_3$ at optimum current.**

The maximum efficiency formulation by CPM (Eq. (6)) is based on the heat balance at the hot and cold sides (Eq. (5)) in which a linear $T$ profile is assumed for the contribution from average Fourier heat flow, see Eq.(10). In the real case involving the temperature dependence of the material properties, the temperature profile due to $\kappa(T)$ is quite different from a linear one and hence $\kappa_{\mathrm{h}}$ and $\kappa_{\mathrm{c}}$ and the corresponding $\frac{dT}{dx}$ are considered to find the heat input or output as in Eq. (3). On a first glance, it could be expected that this might lead to significant error of an efficiency estimate in CPM. However, this is not the case because the temperature profile due to $\kappa(T)$, defined as a partial profile, does not involve any additional source of heat but rather a locally modified $T$ gradient as a response to the local variation of $\kappa$ together with an unchanged constant transmitted Fourier heat flow of the amount $\frac{K\Delta T}{L}$. Overall Fourier heat flow is formed from the net Fourier heat transfer related to the thermal conductance $K$ plus smaller locally varying Fourier heat flow contributions to balance the internally released or absorbed Joule heat plus Thomson heat respectively. In the SpAv+TAv case, the appropriate amounts of pure Fourier heat input and output due to the transferred Fourier heat are calculated, due to spatial averaging of $\kappa$. As the constant $\kappa$ computed using SpAv exactly represents the true thermal conductance (since spatial averaging incorporates the exact temperature distribution), it compensates for not considering different $\kappa(x)$ and the corresponding $\frac{dT}{dx}$ at the hot and cold sides. With that, the replacement of the real Fourier heat flow by $K\Delta T$ in the CPM case is complete and exact.

Likewise, overall Joule heat is correctly estimated by SpAv of $\rho$; however, its distribution to both sides is not anymore ideally symmetric to both sides as in CPM, but is biased by both the

asymmetric release due to spatial dependence of $\rho$ and the asymmetric conduction of (even symmetrically) released Joule heat towards both ends due to spatial asymmetry of $\kappa$ over the element; with that, $Q_{\mathrm{in}}$ and the efficiency calculated by the CPM formula can be slightly inaccurate. Additionally, neglecting Thomson heat in CPM is mainly compensated by considering an averaged $\alpha$ in the Peltier heat input and output calculation, instead of considering $\alpha_h$ and $\alpha_c$ separately. It would be exactly compensated if Thomson heat was symmetrically released to both ends, i.e. in a situation with linear $\alpha(x)$ and symmetric $\kappa(x)$. In any case, the overall Peltier plus Thomson heat balance is correct; merely the location of its appearance is shifted from the interior of the leg (as Thomson heat, in the real case) to the junctions (as Peltier heat, for CPM). However, also here, like for the Joule heat, asymmetric appearance or transmission of Thomson heat may lead to a slightly shifted distribution of the overall unchanged Thomson heat among both ends of the leg in the real case and may thus contribute to the remaining inaccuracy of the CPM result. We note that due to this almost complete compensation, SpAv+TAv averaging provides quite accurate results in efficiency estimation although the underlying CPM temperature profile might be quite far from reality. The remaining 1–1.5% deviation of SpAv+TAv averaging (CPM) from FEM is due to the above mentioned asymmetry[3, 5, 24, 38] of heat generation and distribution due to temperature dependent material properties, which is disregarded by CPM.

According to energy balance, in a temperature dependent case, Thomson heat would be $I(\alpha_h T_h - \alpha_c T_c - \alpha_{\mathrm{TAv}} \Delta T)$ (Thomson heat being the distributed Peltier heat).The difference between Peltier heat balance and thermoelectrically converted electrical power is dissipated (or delivered) across the element as Thomson heat -depending on temperature dependence and current direction. The Thomson part is always smaller than the according Peltier heat. As absorbed Peltier heat will transform into Thomson heat plus electric power, the released Thomson heat is lowered where the power production is higher. Thus, the compensation of the additionally absorbed Peltier heat at the hot side, compared to the CPM case is incomplete by the amount of produced electrical power in the warmer half of the sample above the average and the error in CPM would be proportional to this.

In summary, unless spatial averages are used, conventional averaging methods (like TAv, FMT, MVBT, IWAv) and any correction factors based on just the Thomson and Joule effect [12, 31]

that could be added to CPM, would be insufficient to provide exact results for all material cases and/or for all temperature ranges. This is also evident from the results of Ryu *et al.* [24], where accurate performance estimation is obtained using spatial averages. Additionally, the explained importance of the effect of temperature profile due to $\kappa(T)$ can be seen from the accuracy of 'One-shot approximation' in [24] where $j = 0\,T$ profiles are used. This can be further emphasized by the $j = 0$ temperature profiles (where only $\kappa(T)$ contributes to the $T$ profile shape) of the various materials under consideration here as shown in Figure 7. For a better comparison, normalized $T$ profiles are plotted. For materials with stronger dependence of $\kappa(T)$ such as in SnSe and p-type $Bi_2Te_3$ the TAv fails significantly in predicting the efficiency (see Figure 3a, 17% deviation for SnSe and 5.3% for $Bi_2Te_3$), while for materials with not much varying $\kappa(T)$ such as HMS (2.6 %), $Mg_2Si$ (2.2 %), n-type and p-type $Mg_2(Si,Sn)$ (1.34 % and 0.48 % respectively), the TAv or IWAv predict the performance better (Figure 3a).

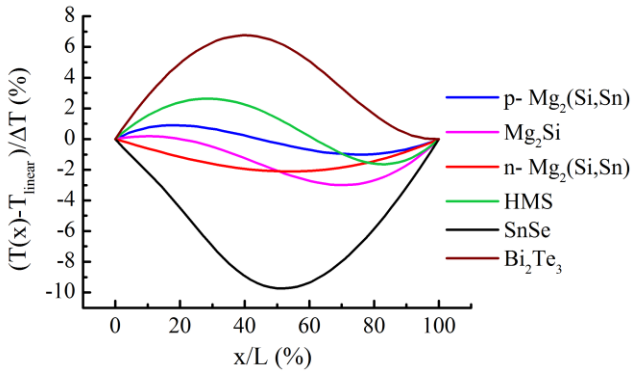


**Figure 7 : Normalised temperature profiles omitting the linear part ($T(x) - T_{lin}$) at zero current for $Bi_2Te_3$, SnSe, p-type $Mg_2(Si,Sn)$, $Mg_2Si$, n-type $Mg_2(Si,Sn)$ and HMS.**

According to Tuley and Simpson [13], the average $zT$ is more important for higher efficiency than the peak $zT$. For typical TE materials the best thermoelectric properties are obtained in the region where minority charge carrier effects start to become relevant. This leads to significant deviation of the thermoelectric properties vs. temperature curves from linearity and hence linear assumptions of $T$ profiles or material properties [24,25] do not hold well anymore. This also implies that the use of temperature averages is not well justified anymore. As for the typical application scenarios, where this temperature region is included or even focused on, the difference between SpAv and TAv is relatively large, see e.g. the p-type $Bi_2Te_3$ case.

# 4 Conclusion

Efficiency estimation by CPM formulae shows that a combination of temperature average for Seebeck and spatial averages for thermal and electrical resistivities, as these represent thermo-voltage, electrical resistance and thermal conductance of the leg physically appropriately, predicts the performance with less error compared to other modes of averaging proposed in the past. The remaining error (0.5–1.5%) is due to the asymmetry in heat generation and transport which is not accounted for in the CPM formulation. A detailed explanation of how the assumption of constant material properties affects the performance calculation and when and why CPM works well or fails was provided. By studying temperature profiles for a representative spectrum of dissimilar materials, a long standing issue of identifying the material specific uncertainty with CPM has been made clear. The $\kappa(T)$ dependence significantly contributes to the bending of the $T$ profile and hence, unless $T$ profiles are taken into account while averaging (i.e. correct spatial averages are involved), the effective resistance values (electrical and thermal) would not be physically appropriate. Therefore, temperature averages which have always been considered to be the easiest method of averaging fail significantly for materials with strongly $T$ dependent thermal conductivity. Neglect of Thomson heat in CPM is mostly compensated by a shift of the Peltier heat calculated at the hot and cold sides, keeping the overall balance of Peltier plus Thomson heat in the leg unchanged. Hence it is not a major issue in CPM as has been considered by previous literatures. Finally, it has to be kept in mind that even though CPM may provide quite accurate performance values with proper choice of averaged properties, the corresponding temperature profile might be inaccurate.

For spatial averages, the exact temperature profile is needed. A fast and simple way of obtaining the temperature profile based on integration by standard table calculation software was presented. By solving the 1D heat balance equation by an iterative numerical procedure, an estimate of individual contributions to the bending of the temperature profile is directly obtained. Visualizing the weight of individual contributions to the bow of the T profile can give an idea to experimentalists how to tune the thermoelectric material properties for better efficiency by manipulating the different heat contributions and their distribution (Joule, Thomson and Fourier heat).

# Acknowledgements

We would like to gratefully acknowledge the endorsement from the DLR Executive Board Member for Space Research and Technology and the financial support from the Young Research Group Leader Program. PP would like to acknowledge the German Academic Exchange Service, DAAD (Fellowship No. 247/2017) for financial support.

APPENDIX

## A. Material data and boundary conditions

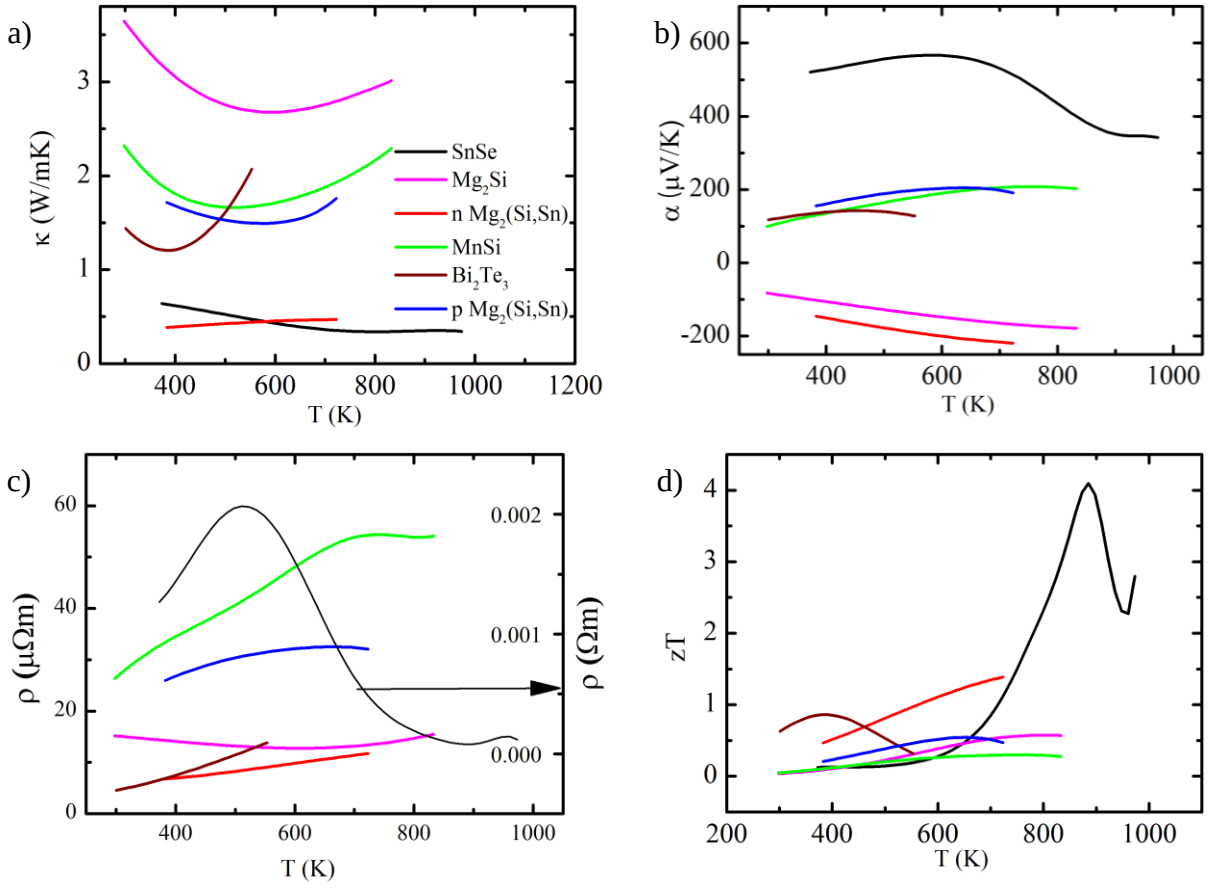


**Figure A.1: Temperature dependent thermoelectric material properties of representative material classes a) Thermal conductivity b) Seebeck coefficient c) Electrical resistivity d) the corresponding *zT*. Since SnSe has high resistivity the scale for it is given on the right *y* axis (indicated by an arrow).**

**Table A.1: Polynomial fit order used for material properties along with the temperature range of analysis for all materials of Fig. A.1**

| Material | Fitted Polynomial degree | Temperature of analysis |
|---|---|---|
| p-$Mg_2(Si,Sn)$ | 5 | 723 K to 383 K |
| n-$Mg_2(Si,Sn)$ | 3 | 723 K to 383 K |
| HMS | 5 | 833 K to 298 K |
| $Mg_2Si$ | 3 | 833 K to 298 K |
| p- $Bi_2Te_3$ | 3 | 553 K to 301 K |
| SnSe | 9 | 973 K to 373 K |

## B. Calculation of the exact temperature profile through integration

The solution procedure is based on the fact that $(T)$ , Joule heat and Thomson heat can be considered as small perturbations contributing to the non-linearity of the temperature profile.

For a slender TEG leg or suitable (symmetrical) boundary conditions (BCs), with no convection or radiation losses, heat flow can be considered to be one-dimensional (1D) which shall be assumed in the following, and the thermoelectric heat balance equation (Eq. 4) in 1D is written as

$$\kappa(T)\frac{\partial^2 T}{\partial x^2}+\frac{d\kappa}{dT}\left(\frac{\partial T}{\partial x}\right)^2-jT\frac{d\alpha}{dT}\frac{\partial T}{\partial x}=-\rho(T)j^2 \tag{B.1}$$

Radiation and convection effects are relevant when a leg is operated at high temperature and open atmosphere and this will reduce the performance of the device significantly. In principle, they can be incorporated mathematically [39-41], although not mathematically strictly in a 1D model. However, these effects can be practically minimized by suitable thermal damping [5] and vacuum conditions, and so they are not considered here.

Assuming that the TE leg is divided mathematically into a large number of segments along the heat flow direction, the individual contributions to the thermal energy balance from each section of a length $dx$ can be calculated according to Eq. (B.1) when the $T$-dependent data is known, provided that an approximated temperature profile $T(x)$ is known initially to deduce its derivatives. In our study, the solution is obtained by a self-consistent iterative procedure starting with a fair initial guess for $T(x)$. Hence, the calculation begins with a simple linear $T(x)$ and since any material property $p(x)=p(T(x))$, $p(x)$ is equivalent in shape to $p(T)$ for the starting iteration. At zero current, Joule heat and Thomson heat are absent and Eq.(B.1) reduces to

$$\frac{d}{dx}\left(-\kappa(x)\frac{dT}{dx}\right)=0 \tag{B.2}$$

Eq. (B.2) indicates that the divergence of Fourier heat flux $q_{\mathrm{F}}(=-\kappa(x)\frac{dT}{dx})$ is zero, implying that no thermal power is converted into electrical power inside the leg and no irreversible or reversible heat is absorbed or released at zero current. The total Fourier heat flux $q_{\mathrm{F}}$ initially can be approximated as $\kappa_{\mathrm{eff}}\Delta T/L$ ($\kappa_{\mathrm{eff}}$ can be obtained as the reciprocal spatial average of $1/\kappa(T)$ and $\Delta T=T_{\mathrm{h}}-T_{\mathrm{c}}$). The temperature profile $T(x)$ can then be found from Eq. (B.2) by spatially integrating $q_{\mathrm{F}}=\kappa_{\mathrm{eff}}\Delta T/L$ , *i.e.,*

$$T(x)_{j=0} = -\kappa_{\text{eff}}\Delta T/L \int_0^x \frac{dx}{\kappa(x)} + C \tag{B.3}$$

Here, the constant of integration $C$ is obtained with the boundary condition $T(x=0) = T_{\text{h}}$. With the $T(x)$ thus calculated, the $\kappa(T(x))$ for the next iteration is obtained and the calculation of Eq. (B.3) is repeated until the solution converges. By this, we have calculated the temperature profile for the open circuit condition ($j = 0$) which is a profile that is bowed only due to $\kappa$ dependence on $T$.

When connected to an external load or current supply $i.e.$, when current flows through the TE leg, the open circuit temperature profile is taken as a first approximation for starting the iterative solution. Rewriting Eq.(B.1) as,

$$\kappa(T)\frac{\boldsymbol{\partial^2 T}}{\boldsymbol{\partial x^2}} = -\frac{d\kappa}{dT}\left(\frac{\boldsymbol{\partial T}}{\boldsymbol{\partial x}}\right)^{\mathbf{2}} + jT\frac{d\alpha}{dT}\frac{\boldsymbol{\partial T}}{\boldsymbol{\partial x}} - \rho(T)j^2\ , \tag{B.4}$$

the right-hand side of Eq. (B.4) is calculated using the temperature profile from the previous step ($T(x)_{j=0}$ for the first step and the $T(x)$ obtained in the subsequent steps, respectively). The left side is solved by integrating spatially twice and solving for the two integration constants $C_1$ and $C_2$ using the BC $T(x=0) = T_h$ and $T(x=L) = T_c$. In summary, let

$$f(x) = -\frac{d\kappa}{dT}\left(\frac{\boldsymbol{\partial T}}{\boldsymbol{\partial x}}\right)^{\mathbf{2}} + jT\frac{d\alpha}{dT}\frac{\boldsymbol{\partial T}}{\boldsymbol{\partial x}} - \rho(T)j^2 \tag{B.5}$$

$$\text{Hence, } \kappa(T(x))\frac{\partial^2 T}{\partial x^2} = f(x),$$

$$\text{Therefore, } T(x)_{j\neq 0} = \int_0^x \int_0^x \frac{f(x)dx}{\kappa(x)}dx + C_1 + C_2$$

This process is repeated until convergence. By following the above procedure, $T$ profiles have been calculated for some of the materials that were used in the CPM section above (Section 2.1). Figure 8 shows the calculated temperature profiles for a TE leg length of 5 mm at $j = 0$ (a and c), $j = j_{\text{opt}}$ (optimum current; Fig. 4b and d) for p-type $Bi_2Te_3$ and for p-type SnSe. $j_{\text{opt}}$ is obtained by calculating the efficiency for different current densities $j$, fitting a polynomial for $\eta$ vs $j$ and finding the point where $\frac{d\eta}{dj}$ becomes zero; i.e, the current density where the efficiency is maximum. Since the TE properties of SnSe have a complex temperature dependence, 8$^{\text{th}}$ and 9$^{\text{th}}$ order polynomial fits were used for fitting the material properties.

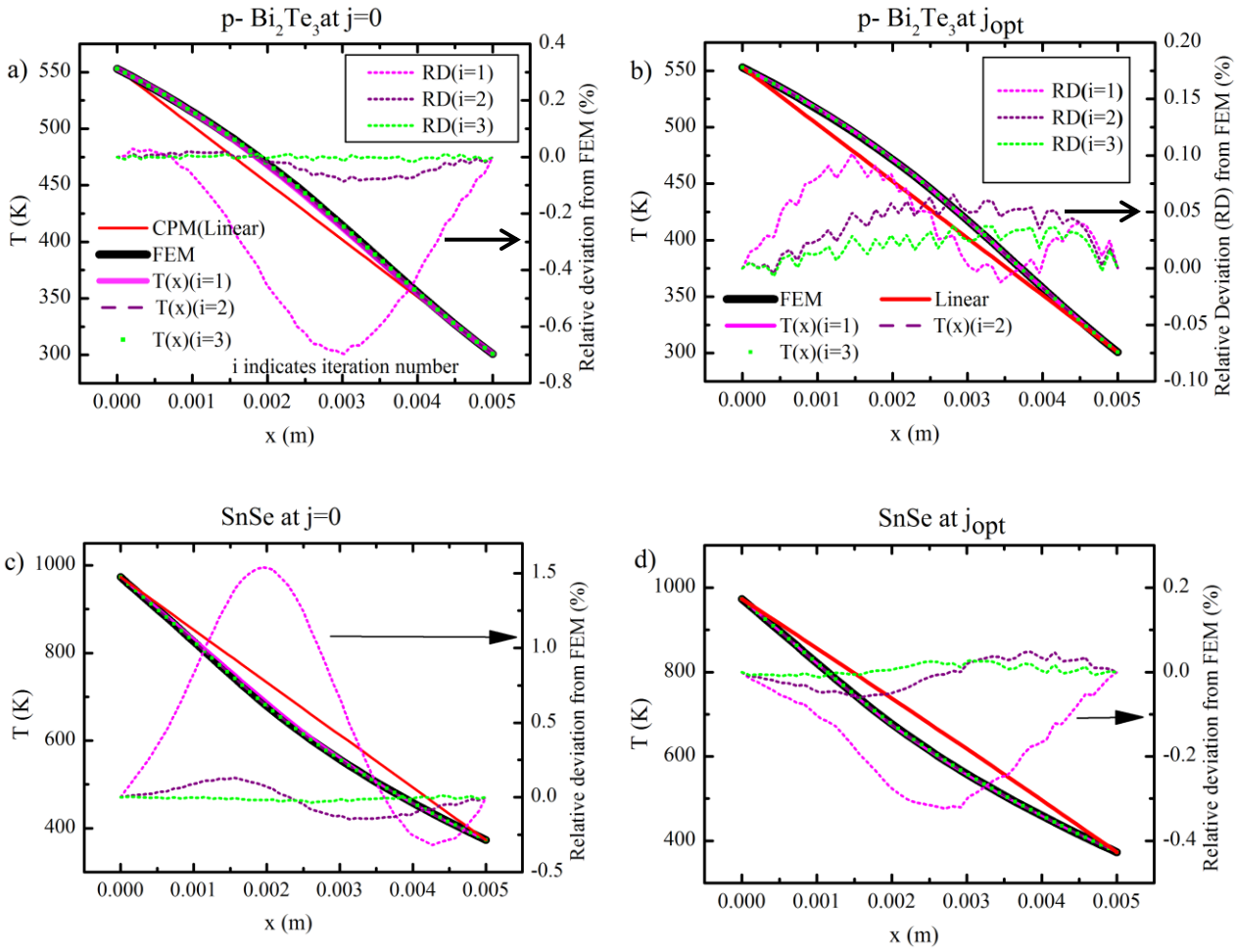


**Figure 8: Calculated T profiles for p-type $Bi_2Te_3$ at a) $j = 0$ and b) $j = j_{opt}$ and for p-type SnSe (legend same as that of $Bi_2Te_3$) at c) $j = 0$ and d) $j = j_{opt}$ for the first three iterations. The dashed lines represent the relative difference between FEM T profile and the T profiles calculated using the iterative method.**

Conventionally, perturbation solution is obtained using Taylor or Maclaurin series [25-27] expansion and this very fact makes the solution convergent. Consequently, these traditional methods require parameterization and complicated analytical computation [38]. A brief mathematical description on the application of perturbation theory specifically to thermoelectrics can be found in Wee [25]. In this work, Wee assumes 2$^{nd}$ order polynomials for a particular material case and obtains the solution using series expansion. On a similar work, Ju *et al.* [26] derived analytical expressions for the temperature profile for another particular material case assuming parabolic functions for material properties. Later, Zhang [38] provided a more generalized solution based on the Homotopy perturbation method in an effort to signify the

importance of temperature dependence of material properties. Recently, Marchenko [27] provided a comparison between using quadratic and linear approximations in perturbation theory.

In our case, the convergence of the solution is ensured by spatial integration, which is mathematically equivalent to summing up the individual terms of the series. In this study, integration was done using trapezoidal rule in-built in the software Origin 8.5.1. In perturbation theory, the closer the starting function, the faster the convergence of the solution. Hence, the current method which inputs the temperature profile from previous step is convergent in two or three iterations as can be seen from the very low relative deviation (right side *y* axis) of the third iteration from the exact *T* profile (FEM) even for strongly *T* dependent materials as in Figure 8. In doing so, the calculation times are reduced tremendously compared to FEM and individual heat contributions can be easily visualized by integrating the corresponding terms in the heat balance equation.

# Bibliography


1. Snyder, G.J. and E.S. Toberer, *Complex thermoelectric materials*, in *Materials For Sustainable Energy: A Collection of Peer-Reviewed Research and Review Articles from Nature Publishing Group*. 2011, World Scientific. p. 101-110.
2. Rowe, D.M., *Thermoelectrics handbook: macro to nano*. 2005, CRC press.
3. *A.F. Ioffee. Semiconductor thermoelements and thermoelectric cooling.London, Infosearch, ltd., 1957.*
4. Antonova, E.E. and D.C. Looman. *Finite elements for thermoelectric device analysis in ANSYS*. in *Thermoelectrics, 2005. ICT 2005. 24th International Conference on*. 2005. IEEE.
5. Goupil, C., *Continuum theory and modeling of thermoelectric elements*. 2015: John Wiley & Sons.
6. Kim, C.N., *Development of a numerical method for the performance analysis of thermoelectric generators with thermal and electric contact resistance.* Applied Thermal Engineering, 2018. **130**: p. 408-417.
7. Hogan, T. and T. Shih, *Modeling and characterization of power generation modules based on bulk materials.* Thermoelectrics Handbook: Macro to Nano, 2006: p. 12.1-12.23.
8. Oliveira, K.S., R.P. Cardoso, and C.J. Hermes, *Two-Dimensional Modeling of Thermoelectric Cells.* 2014.
9. Sherman, B., R. Heikes, and R. Ure Jr, *Calculation of efficiency of thermoelectric devices.* Journal of Applied Physics, 1960. **31**(1): p. 1-16.
10. Brandt, J.A., *Solutions to the differential equations describing the temperature distribution, thermal efficiency, and power output of a thermoelectric element with variable properties and cross sectional area.* Advanced Energy Conversion, 1962. **2**: p. 219-230.
11. Lee, H., et al., *Modeling and analysis of the effect of thermal losses on thermoelectric generator performance using effective properties.* Applied Energy, 2018. **211**: p. 987-996.
12. Kim, H.S., et al., *Relationship between thermoelectric figure of merit and energy conversion efficiency.* Proceedings of the National Academy of Sciences, 2015. **112**(27): p. 8205-8210.
13. Tuley, R. and K. Simpson, *ZT Optimization: An Application Focus.* Materials, 2017. **10**(3): p. 309.
14. Armstrong, H., et al., *Estimating Energy Conversion Efficiency of Thermoelectric Materials: Constant Property Versus Average Property Models.* Journal of Electronic Materials, 2017. **46**(1): p. 6-13.
15. Lau, P.G. and R.J. Buist. *Calculation of thermoelectric power generation performance using finite element analysis*. in *Thermoelectrics, 1997. Proceedings ICT'97. XVI International Conference on*. 1997. IEEE.
16. Mahan, G., *Inhomogeneous thermoelectrics.* Journal of Applied Physics, 1991. **70**(8): p. 4551-4554.
17. Fraisse, G., et al., *Comparison of different modeling approaches for thermoelectric elements.* Energy conversion and management, 2013. **65**: p. 351-356.

18. Chen, J., Z. Yan, and L. Wu, *The influence of Thomson effect on the maximum power output and maximum efficiency of a thermoelectric generator*. Journal of Applied Physics, 1996. **79**(11): p. 8823-8828.
19. Huang, M.-J., R.-H. Yen, and A.-B. Wang, *The influence of the Thomson effect on the performance of a thermoelectric cooler.* International Journal of Heat and Mass Transfer, 2005. **48**(2): p. 413-418.
20. Sandoz-Rosado, E.J., S.J. Weinstein, and R.J. Stevens, *On the Thomson effect in thermoelectric power devices.* International Journal of Thermal Sciences, 2013. **66**: p. 1-7.
21. Lee, H., *The Thomson effect and the ideal equation on thermoelectric coolers.* Energy, 2013. **56**: p. 61-69.
22. Yamashita, O., *Effect of linear temperature dependence of thermoelectric properties on energy conversion efficiency*. Energy conversion and management, 2008. **49**(11): p. 3163-3169.
23. Yamashita, O., *Effect of linear and non-linear components in the temperature dependences of thermoelectric properties on the cooling performance.* Applied Energy, 2009. **86**(9): p. 1746-1756.
24. Ryu, B., J. Chung, and S. Park, *Thermoelectric efficiency has three Degrees of Freedom.* arXiv preprint arXiv:1810.11148, 2018.
25. Wee, D., *Analysis of thermoelectric energy conversion efficiency with linear and nonlinear temperature dependence in material properties.* Energy conversion and management, 2011. **52**(12): p. 3383-3390.
26. Ju, C., et al., *Revisiting the temperature dependence in material properties and performance of thermoelectric materials.* Energy, 2017. **124**: p. 249-257.
27. Marchenko, O.V., *Performance modeling of thermoelectric devices by perturbation method.* International Journal of Thermal Sciences, 2018. **129**: p. 334-342.
28. Fraisse, G., et al., *Study of a thermoelement's behaviour through a modelling based on electrical analogy.* International Journal of Heat and Mass Transfer, 2010. **53**(17-18): p. 3503-3512.
29. Seifert, W., M. Ueltzen, and E. Müller, *One-dimensional modelling of thermoelectric cooling.* physica status solidi (a), 2002. **194**(1): p. 277-290.
30. Sunderland, J.E. and N.T. Burak, *The influence of the Thomson effect on the performance of a thermoelectric power generator.* Solid-State Electronics, 1964. **7**(6): p. 465-471.
31. Min, G., D.M. Rowe, and K. Kontostavlakis, *Thermoelectric figure-of-merit under large temperature differences.* Journal of Physics D: Applied Physics, 2004. **37**(8): p. 1301.
32. Kim, H.S., W. Liu, and Z. Ren, *The bridge between the materials and devices of thermoelectric power generators.* Energy & Environmental Science, 2017. **10**(1): p. 69-85.
33. Snyder, G.J. and T.S. Ursell, *Thermoelectric efficiency and compatibility.* Physical review letters, 2003. **91**(14): p. 148301.
34. Sankhla, A., et al., *Mechanical Alloying of Optimized Mg2 (Si, Sn) Solid Solutions: Understanding Phase Evolution and Tuning Synthesis Parameters for Thermoelectric Applications.* ACS Applied Energy Materials, 2018. **1**(2): p. 531-542.
35. Kamila, H., et al., *Analyzing transport properties of p-type Mg 2 Si–Mg 2 Sn solid solutions: optimization of thermoelectric performance and insight into the electronic band structure.* Journal of Materials Chemistry A, 2019.

36. Kim, H.S., et al., *Design of segmented thermoelectric generator based on cost-effective and light-weight thermoelectric alloys.* Materials Science and Engineering: B, 2014. **185**: p. 45-52.
37. Zhao, L.-D., et al., *Ultralow thermal conductivity and high thermoelectric figure of merit in SnSe crystals.* Nature, 2014. **508**(7496): p. 373.
38. Zhang, T., *Effects of temperature-dependent material properties on temperature variation in a thermoelement.* Journal of Electronic Materials, 2015. **44**(10): p. 3612-3620.
39. Muto, A., et al., *Thermoelectric properties and efficiency measurements under large temperature differences.* Review of Scientific Instruments, 2009. **80**(9): p. 093901.
40. Meng, F., L. Chen, and F. Sun, *A numerical model and comparative investigation of a thermoelectric generator with multi-irreversibilities.* Energy, 2011. **36**(5): p. 3513-3522.
41. Li, T., et al., *Thermoelectric properties and performance of flexible reduced graphene oxide films up to 3,000 K.* Nature Energy, 2018. **3**(2): p. 148.